Demonstration of a NOR logic gate using a single molecule and two surface gold atoms to encode the logical input

W.-H. Soe,[1,*] C. Manzano,[1] A. De Sarkar,[1] F. Ample,[1] N. Chandrasekhar,[1] N. Renaud,[2,*] P. de Mendoza,[3] A. M. Echavarren,[3] M. Hliwa,[4,5] and C. Joachim[1,4]

[1]*IMRE, A*STAR (Agency for Science, Technology and Research), 3 Research Link, 117602 Singapore*

[2]*Department of Chemistry, Northwestern University, 2145 Sheridan Road, Evanston, Illinois 60208-3113, USA*

[3]*Institut of Chemical Research of Catalonia (ICIQ), Av. Països Catalans 16, E-43007 Tarragona, Spain*

[4]*CEMES & MANA Satellite, CNRS, 29 rue J. Marvig, F-31055 Toulouse Cedex, France*

[5]*Faculté des Sciences Ben M'Sik, Université Hassan II_Mohammedia, B.P. 7955 Sidi Othman, Casablanca, Morroco*

(Received 8 October 2010; revised manuscript received 23 December 2010; published 26 April 2011)

A logic gate has been implemented in a single trinaphthylene molecule. Each logical input controls the position of a surface Au atom that is brought closer or further away from the end of one of the naphthyl branch. Each Au atom carries 1 bit of information and is able to deform nonlocally and to shift in energy the molecular electronic states of the trinaphthylene. Probed at the end of the third naphthyl branch using scanning tunneling spectroscopy, the variations of the tunneling current intensity as a function of the Au atoms position measures the logical output of the gate. We demonstrate both theoretically and experimentally that these variations respect the truth table of a NOR logic gate.

DOI: 10.1103/PhysRevB.83.155443 PACS number(s): 85.65.+h, 03.67.−a, 07.79.Fc, 85.35.−p

I. INTRODUCTION

Logic gates are the building block of modern electronic architecture and are ubiquitously found in any electronic circuit whose purpose is to perform a given arithmetic operation. The computing power by surface area is therefore highly dependent on the minimal surface required to implement a given logic function. To improve this computing power, one can scale down classical circuits, either improving lithography techniques[1] or using tailor-made materials.[2] However, to overcome the foreseeable difficulties limiting this miniaturization down to the atomic scale, new electronic architectures have to be developed. Among many other solutions, molecular electronics is an interesting approach.[3]

In this frame, many solutions have been proposed to design a small computing unit out of a few molecules.[4] Logic gates have been constructed using the domino-like cascading of CO molecules to perform the logic operation.[5] Intramolecular proton transfer can also be used to induce a topological rotation in the frontier orbitals of a naphthalocyanine molecule that influences the electronic states of neighboring molecules.[6,7] Molecular cellular automata is another promising solution where the flow of information propagates along a molecular network by changing the charge state of each molecule.[8]

Turning a single molecule into a logic circuit is a more delicate problem. The obvious solution of shaping the molecule like the corresponding circuit[9] suffers from an important drawback: the decay of the current intensity passing through the molecule with its length.[10] Alternative solutions have been proposed to turn the quantum properties of a single molecule to our advantage. Stimulated Raman adiabatic passage can thus be used on a few level system to implement sequential arithmetic operations.[11] Quantum interferences[12] or negative differential resistance[13] are other quantum effects that can be used to implement logic devices. In this article we follow the quantum Hamiltonian computing (QHC) approach to design a logic gate in a model system and implement it experimentally in a single molecule. We would like to stress that the QHC approach is not qubit based and deals with classical Boolean functions. It nevertheless uses quantum properties of the system, that is, the nonlocal deformation of its delocalized eigenstates, to implement a Boolean function. However it does not rely explicitly on the superposition principle to encode the logical input, as it is the case in a standard qubit-based quantum computation approach.[14]

The QHC approach proposes to encode the logical inputs in the Hamiltonian of the molecule and the logical output in the tunneling current intensity passing through a part of the molecule.[15,16] The basis of this approach is described in Sec. II using a model seven-state quantum system whose Hamiltonian depends on two logical inputs. Modifying the delocalized eigenstates of the system, each logical input acts nonlocally on its electronic conductance. Switching one logical input at one end of the system can induce strong modification of its conductance at the other end. This is very different from the very local action that a classical switch has on the conductance of an electronic circuit. The corresponding scanning tunneling microscopy (STM) experimental setup is presented in Sec. III. Controlling the position of two surface Au atoms in the vicinity of a trinaphthylene molecule physisorbed on a Au(111) substrate, a digital logic gate implementing the logical negation NOR operation of the OR Boolean operator is realised. Each Au is approached or moved away from one of the three naphtyl branches while the current going from the tip to the substrate through the end of the third naphtyl branch is recorded. Connecting an Au at one end of the molecule strongly perturbs its conductance and therefore induces a modification of the tunneling current intensity. Quantum chemistry calculations of the valence molecular orbitals and the multiconfiguration electronic states of the trinaphthylene molecule interacting with either zero, one, or two Au atoms are presented in Sec. IV. These calculations provide insight into the mechanism of this molecular logic gate and reveal its connection with the model system of Sec. II. These results indicate a method for the future design of complex Boolean logic gates using a single molecule.

 ©2011 American Physical Society

II. THE QHC DESIGN OF A NOR LOGIC GATE

Many methods exist to calculate the electronic conduction of a quantum system inside a tunneling junction.[17] However, the analytical expression provided by these methods are quite difficult to handle even for simple quantum systems. This complexity is a major obstacle in developing a simple theory of the response of a quantum system to a modification of its Hamiltonian.

Following a recently proposed approach,[18] the electronic conductance can be calculated from the temporal evolution of the wave vector from one eigenstate of one electrode to an eigenstate of the other electrode. The two scattering eigenstates must have the same energy E. It has been demonstrated that the value of the transmission coefficient at the energy E, noted $T(E)$, is proportional to the square of the oscillation frequency Ω between the two scattering eigenstates of energy E.[19] In this picture let us consider the model seven-state system whose Hamiltonian is given by:

$$\mathcal{H} = \begin{array}{c} \begin{array}{ccccccc} |\phi_{\rm tip}\rangle & |\phi_{\rm sub}\rangle & |m_1\rangle & |m_2\rangle & |m_3\rangle & |1\rangle & |2\rangle \end{array} \\ \left(\begin{array}{cc|ccccc} E & . & \varepsilon & . & . & . & . \\ . & E & \varepsilon & . & . & . & . \\ \hline \varepsilon & \varepsilon & e & k & k & . & . \\ . & . & k & e & k & \alpha & . \\ . & . & k & k & e & . & \beta \\ . & . & . & \alpha & . & e & . \\ . & . & . & . & \beta & . & e \end{array}\right) \end{array} \qquad (1)$$

and represented in Fig. 1(a). The zero matrix elements of the Hamiltonian are represented by dots to emphasize the structure of the system. The states $|\phi_{\rm tip}\rangle$ and $|\phi_{\rm sub}\rangle$ are the two scattering eigenstates of the electrodes, and are labeled tip and sub, to anticipate the STM implementation used in Sec. III where one electrode is the tip of the STM and the other the substrate. Due to the delocalization of $|\phi_{\rm tip}\rangle$ and $|\phi_{\rm sub}\rangle$ over the electrodes, their interaction with the central system remains very weak and is here taken as $\varepsilon = 10^{-2}$ eV. The states $|m_1\rangle$, $|m_2\rangle$, and $|m_3\rangle$ constitute the board of this simplified molecule. The coupling strengths between the states $|1\rangle$, $|2\rangle$ and this board are used to encode the logical inputs. These latter are noted α and β: α is the coupling strength between the states $|m_2\rangle$ and $|1\rangle$ and β is the coupling strength between the states $|m_3\rangle$ and $|2\rangle$. These two input parameters can take the values of 0 or 1. Changing either of these two coupling strengths changes all the eigenstates and eigenenergies of the Hamiltonian. Therefore the logical inputs control the current intensity going from $|\phi_{\rm tip}\rangle$ to $|\phi_{\rm sub}\rangle$ even if these two states are only connected to $|m_1\rangle$. Initially prepared on $|\phi_{\rm tip}\rangle$, the state vector $|\psi(t)\rangle$ evolve in time exploring the state space of the system following the solution of the time-dependent Schrodinger equation (TDSE): $|\psi(t)\rangle = \exp(-i\mathcal{H}\frac{t}{\hbar})|\phi_{\rm tip}\rangle$. Due to the weak values of ε, the population of the $|\phi_{\rm sub}\rangle$: $\mathcal{P}_{\rm sub}(t) = |\langle\phi_{\rm sub}|\psi(t)\rangle|^2$, oscillates smoothly driven by a single secular oscillatory term whose oscillation frequency is Ω. The Lowdin partitioning[20] allows us to derive an analytical expression for Ω that depends on the value of the logical inputs. Discretizing this expression over the binary values of α and β leads to an approximate expression of Ω that associates Dirac distributions and Boolean operators:

$$\begin{aligned} \Omega(E,\alpha,\beta) = {} & \overline{\alpha+\beta}\ \delta(\Delta^4 - 3k^2\Delta^2 - 2k^3\Delta) \\ & + \alpha \oplus \beta\ \delta[\Delta^4 - (1+3k^2)\Delta^2 - 2k^3\Delta + k^2] \\ & + \alpha\cdot\beta\delta[\Delta^4 - (2+3k^2)\Delta^2 - 2k^3\Delta + 2k^2 + 1] \end{aligned} \qquad (2)$$

with $\Delta = E - e$. The Dirac distributions in Eq. (2) comes from the perturbative nature of the Lowdin partitioning and the pole of the corresponding effective Hamiltonian.[21] Tuning the value of Δ allows us to cancel out one or several arguments of the Dirac distributions in Eq. (2) and to select the associated Boolean operators. Depending on which operators have been selected, a given Boolean function is implemented in the system. The case of the NOR gate is given by $\Delta = 2k$. For this value of Δ, the argument of the first Dirac distribution cancels out unlike the other ones. This selects the operator $\overline{\alpha+\beta}$ and leads to $\Omega(\alpha,\beta) \propto \overline{\alpha+\beta}\ \delta(0)$. The oscillation frequency is then maximum for $\overline{\alpha+\beta} = 1$, that is, if $\alpha = \beta = 0$, and very small otherwise. To confirm this analysis the TDSE has been solved numerically for $E = -1$ eV, $e = 0$ eV, $k = -1/2$ eV, and $\varepsilon = 0.01$ eV. The evolution of $\mathcal{P}_{\rm sub}(t)$ is represented in Fig. 1(b) for the different values of α and β. In the case

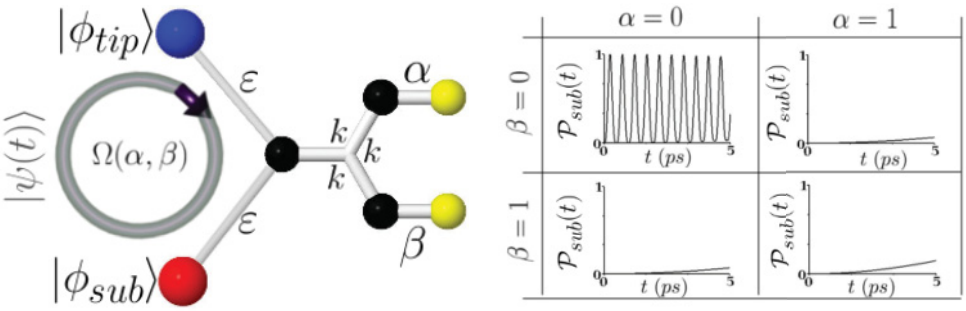

(a) (b)

FIG. 1. (Color online) (a) Graphical representation of the system described by the Hamiltonian (1). $|\phi_{\rm tip}\rangle$ and $|\phi_{\rm sub}\rangle$ are eigenstates of the two electrodes. The logical input are encoded in the value of α and β. (b) Population of $|\phi_{\rm sub}\rangle$ for $E = -1$ eV, $e = 0$ eV, $k = -1/2$ eV, and $\varepsilon = 10^{-2}$ eV. When $\alpha = \beta = 0$ an eigenstate of the system has the same energy as $|\phi_{\rm tip}\rangle$ and $|\phi_{\rm sub}\rangle$. This leads to a maximum oscillation frequency. This is not the case for the other values of the logical input and consequently the oscillation frequency is much lower. The QHC design plays with the level-repulsion effect for some molecular states to be at or off resonance with the initial and target state.

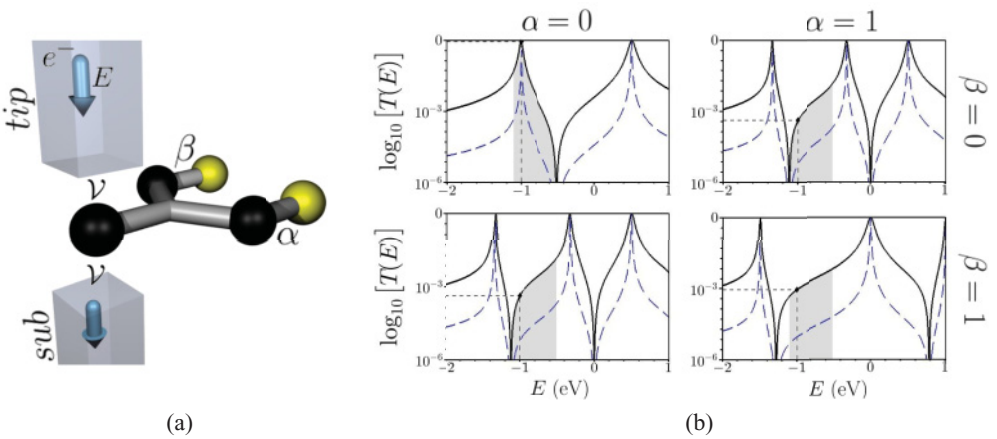

(a) (b)

FIG. 2. (Color online) (a) Simplified QHC molecule inserted between two electrodes. The two electrodes are supposed to interact only with the first state of the simplified molecule through the couplings $\mathcal{V}$. These couplings are $\mathcal{V} = -0.15$ eV. (b) The transmission coefficient of the system represented in (a) calculated with the ESQC technique for different values of the logical input (solid black line). The $T(E)$ follows the same variation as the normalized oscillation frequency for the system represented in Fig. 1(a) (dashed blue line). The chemical potentials of the electrode define the integration region of the $T(E)$ (grey shaded area) that gives the output current intensity.

$\alpha = \beta = 0$, $\mathcal{P}_{\text{sub}}(t)$ oscillates smoothly from $|\phi_{\text{tip}}\rangle$ to $|\phi_{\text{sub}}\rangle$ with a frequency of 6.45 THz. In the other cases, the oscillation frequency is much lower and drops to 0.05 and 0.07 THz for $\alpha \neq \beta$ and $\alpha = \beta = 1$, respectively. The high frequency obtained for $\alpha = \beta = 0$ is due to the presence of an eigenstate of the central system with an energy E that connects $|\phi_{\text{tip}}\rangle$ and $|\phi_{\text{sub}}\rangle$. The energy of this resonant eigenstate is shifted out of the resonance for nonnull values of the logical inputs and the oscillation frequency decreases dramatically due to the weak value of ε.

When the central system is inserted between two electrodes [Fig. 2(a)], the transmission coefficient at the energy E is proportional to the square of the oscillation frequency Ω determined above. This equivalence is illustrated in Fig. 2(b) where these two quantities present the same line shape with the usual resonance and interference patterns. The $T(E)$ spectra has been calculated with the elastic scattering quantum chemistry (ESQC) technique.[22] Each contacting electrode was modeled by a linear chain with a zero on-site energy and a site to site coupling of -2 eV. The coupling $\mathcal{V}$ between the last site of each electrode and the state $|m_1\rangle$ has been set to 0.15 eV. This last parameter controls the width of the resonances that are broaden when $\mathcal{V}$ increases. The weak value used here leads to sharp resonances. The electronic conductance of the system at $E = -1$ eV is resonant, that is, $T(-1\text{ eV}) = 1$, for $\alpha = \beta = 0$ and nonresonant, that is, $T(-1\text{ eV}) \simeq 0$, for the other logical input values. This is exactly what is predicted by Eq. (2). Consequently the output status of the logic gate is given by the value of the electronic conductance of the system at this precise energy to obtain the NOR gate. However it is more stable to access the output status using the current intensity going through the system rather than its spectral conductance.

Following the Landauer-Buttiker approach, this intensity is obtained integrating the transmission coefficient between the chemical potentials of the two electrodes. These chemical potentials depend mainly on the Fermi energy of the electrodes and the applied bias voltage. The chemical potential are simply set here at -1.1 eV for the tip and -0.5 eV for the substrate. They define the integration region represented by a grey shaded area in Fig. 2(b). To illustrate the mechanism underlying our approach let us consider Fig. 3(a) where the changes of the system's eigenstates induced by α are represented (β remaining equal to 0 for simplicity). The eigenstates are represented supposing that each state correspond to a p_z orbital. When $\alpha = 0$, the lowest lying eigenstate (called HOMO for simplicity) is located at $E = -1$ eV. Responsible for the resonance observed at $T(-1\text{ eV})$ for $\alpha = \beta = 0$, this state lies between the chemical potential of the two electrodes [grey shaded area in Figs. 2(b) and 3(a)]. Due to this available tunneling channel, the current intensity flowing through the system [solid green line in Fig. 3(a)] is quite strong: 1.5 μA. When α increases the LUMO state [dashed red line in Fig. 3(a)] pushed the HOMO down in energy. When α is strong enough to push the HOMO out of the integration region, the current intensity drops to almost zero. The same analysis can be made when both α and β vary from 0 to 1 [Fig. 3(b)]. As long as the HOMO remains in the integration region the current intensity is strong and drops to zero otherwise. The width of the HOMO, and consequently the value of $\mathcal{V}$, controls the steepness of the transition to go from a 0 to a 1 logical output. For large $\mathcal{V}$, the broad resonances lead to a smooth transition. On the contrary, a small $\mathcal{V}$ leads to sharp resonances and gives a steeper transition. In this latter case the output intensity surface presents large stability regions at its corner. This leads to a self-correction of small deviations in the value of the logical inputs that induce even smaller deviations in the output status. The values of all the physical quantities relative to the logical output status are summarized in the last part of Fig. 3(b) for the four different values of the logical input.

III. A LT-UHV STM IMPLEMENTATION OF THE NOR GATE

Due to its star-like topology, similar to the model system presented in Sec. II, a trinaphthylene molecule [see Fig. 4(a)]

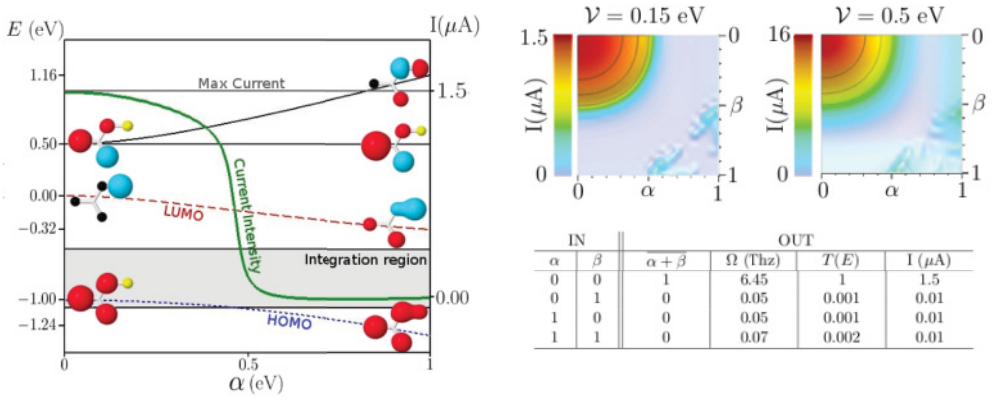

IN		OUT			
α	β	$\alpha+\beta$	Ω (Thz)	$T(E)$	I (μA)
0	0	1	6.45	1	1.5
0	1	0	0.05	0.001	0.01
1	0	0	0.05	0.001	0.01
1	1	0	0.07	0.002	0.01

(a) (b)

FIG. 3. (Color online) (a) Impact of α on the system's eigenstates indicated by the dotted blue, dashed red, and solid black curves. When $\alpha = 0$ the HOMO lies between the chemical potential of the two electrodes that defines the integration region (grey shaded area) leading to a strong current intensity. If α is strong enough to push the HOMO out of the integration region, the current intensity drop to almost zero. (b) Current intensity when α and β vary from 0 to 1. The smaller $\mathcal{V}$, the steepest the transition goes from a 1 to a 0 output. Values of the different physical quantities relative to the output status for the four input configurations.

is a good candidate to go from the theoretical design of Sec. II to a realistic experiment. This STM experimental setup is presented in Fig. 4(a). A trinaphthylene molecule is physisorbed on an Au(111) surface to preserve the integrity of its molecular electronic states. Besides, this physisorption allows us to have a large enough space between the molecular board and the surface where surface Au atoms can be slid into contact with the π network of the trinaphthylene. Each logical input, α and β, controls the position of one Au atom around the end of a given naphtyl branch. If $\alpha = 0$, the corresponding Au atom is moved away from the molecule and does not perturb its molecular electronic states. On the contrary, when $\alpha = 1$, this Au atom is STM manipulated toward the end of a naphtyl branch and perturbs all the electronic states of the trinaphthylene. The value of β controls similarly the position of a second Au atom at the end of a second naphtyl branch. The logical output is recorded by the tunneling current intensity going from the tip to the substrate through the end of the third naphtyl branch.

As demonstrated below, the variations of the tunneling current intensity with the position of the Au atoms respect the truth table of a NOR logic gate. These variations are caused by a local electronic perturbation of the molecule that occurs far away from the region where its conductance is probed. If they were acting classically, the gold atoms would only perturb the electronic conduction of the molecule in their immediate

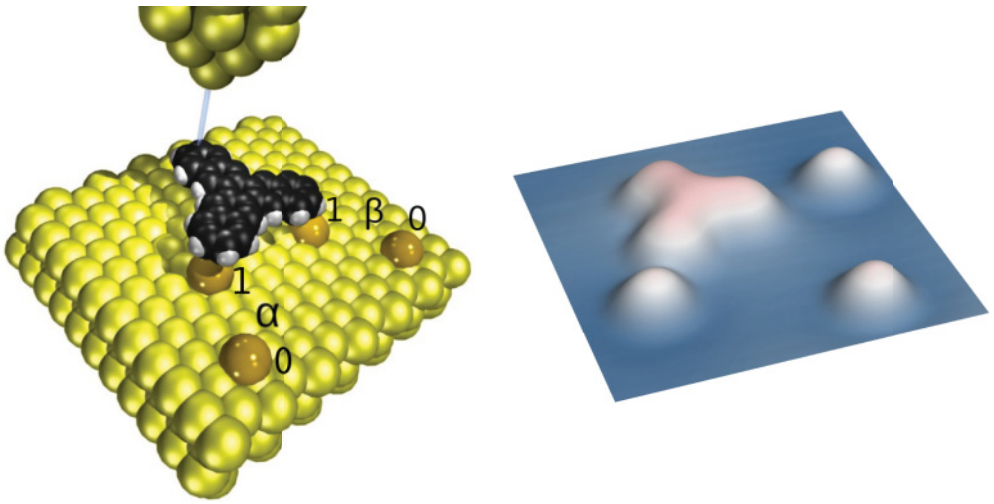

(a) (b)

FIG. 4. (Color online) (a) The STM experimental setup used in this article. The trinaphthylene is physisorbed on Au(111). Each logical input, denoted α and β, controls the position of a given surface Au atom. When $\alpha = 0$ the corresponding Au atom is moved away from the molecule. On the contrary when $\alpha = 1$, this atom is STM manipulated toward the end of a naphtyl branch. β controls the second Au atom in the same way. The output of this molecular logic gate is measured in the tunneling current intensity going from the tip to the substrate through the end of the third naphtyl branch. (b) Constant current STM experimental image of the trinaphthylene physisorbed on Au(111) with three Au atoms in its surrounding (scale: 4 nm $\times$ 4 nm).

surrounding. But due to the delocalization of the molecular orbitals over the molecular board, each Au atom is able to act nonlocally on the molecule and have a remote action on its electronic conductance.[23]

Analytically pure trinaphthylene has been synthesized from 3-trimethylsilylnaphthyl-2- trifluoromethanesulphonate via a palladium-catalyzed [2+2+2] trimerization.[24,25] Once synthesized, the molecules have been sublimed by free evaporation in an UHV preparation chamber on a Au(111) surface kept at room temperature. Thereafter, the Au(111) sample was cooled down to 5 K. With the evaporation parameters used, coverage under 0.1 monolayer was attained. STM imaging shows molecules adsorbed on Au terraces and at step edges. Single Au atoms were produced by a gentle crash of the W tip apex on the Au(111) surface and manipulated with the STM tip for contacting a single molecule.[26] A typical image of a trinaphthylene molecule with three companion single Au atoms is presented in Fig. 4(b). For this image three Au atoms were STM manipulated in close proximity to a molecule: two for the logical inputs and one as a reference to verify whether the molecule moved during the STM manipulation of a given Au atom. Standard $R = 250$ MΩ low bias voltage tunneling resistance was used for imaging and $R = 0.2$ MΩ for single Au atom manipulation in pulling mode. Whenever necessary, the trinaphthylene molecule was manipulated to bring it closer to the Au atoms, also in pulling mode, using an $R = 200$ MΩ junction resistance with a large bias voltage. To reset the two logical inputs to zero, the trinaphtylene can be easily manipulated away from the two Au atoms in a pushing mode.

The three nonequivalent input configurations, that is, (0,0), (1,0), and (1,1), are presented in Fig. 5 with none, one, and two Au atoms interacting with the trinaphthylene molecule. In each case, the final molecule conformation and the position of the Au atoms at the end of the naphthyl branches were determined by comparing experimental and calculated STM-elastic scattering quantum chemistry images.[22] The atomic superposition and electron delocalization (ASED+)[27,28] molecular mechanics routine was used to extract the optimum molecule-surface conformation so that the experimental and calculated images converge. As it can be seen in Fig. 5, these calculations reveal that contacting one Au atom to the end of a naphthyl branch deforms its terminal phenyl group while slightly lifting up the corresponding hydrogen atom.[23]

The tunneling current intensity through the third branch of the molecule is highly sensitive to the energy position and the lateral expansion of the trinaphtylene's electronic states. To understand how the manipulation of the Au atoms affects these molecular electronic states, dI/dV maps of the trinaphthylene molecule has been recorded for zero, one, and two gold atoms interacting with the molecule. These maps, presented in Fig. 6, allow us to visualize the lateral spatial extension of the frontier orbitals of the trinaphthylene for the different value of the

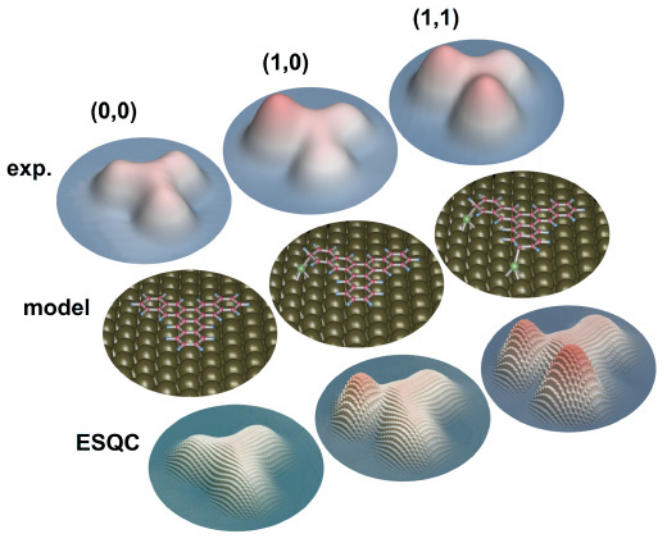

FIG. 5. (Color online) Top: The three experimental images obtained approaching successively none, one, and two Au atoms near the end of the naphtyl branches. Middle: Molecular model of the Au-trinaphthylene surface system when optimizing its atomic scale surface structure for the experimental and calculated images to converge scan by scan. This optimization demonstrates the displacement of the H atoms when approaching a Au atom to the molecule. Bottom: The theoretical ESQC-STM images of the trinaphtylene interacting with none, one, and two surface atoms.

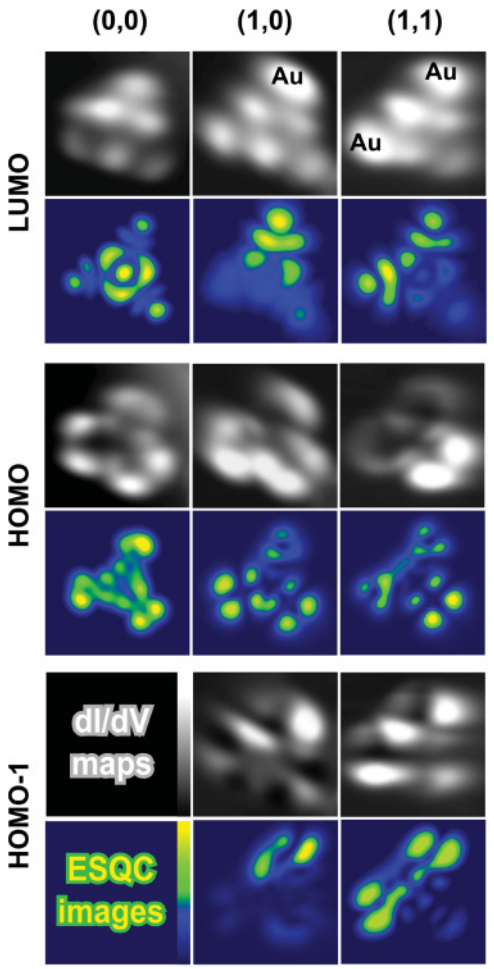

FIG. 6. (Color online) Experimental and theoretical dI/dV map of the molecule recorded at the energy of the HOMO-1, HOMO, and LUMO of the system for zero, one, and two atoms interacting with the molecule. A good agreement is seen between experiment and theory. Experimental and theoretical images shows how approaching one atom in the vicinity of the molecule deforms nonlocally its molecular orbitals due to their delocalization over the molecular board.

logical input. ESQC STM image calculations clearly identify the corresponding molecular orbitals of the trinaphthylene. The case where no Au atoms are connected to the molecule, that is, $\alpha = \beta = 0$, allows us to determine precisely the optimum tip position above the third naphtyl branch. In this (0,0) case, the HOMO presents two lobes roughly localized on the two first carbon atoms of the third naphtyl branch. Since a strong current is desired for the (0,0) input configuration, the tip apex has been experimentally positioned on top of one of these two lobes. Contacting Au atoms to the trinaphthylene deforms its electronic states not only in the vicinity of the Au atoms but all over the molecular board. The value of the logical inputs are quantum mechanically distributed over the molecule instead of being only available near its contact points with the Au atoms.

The different dI/dV spectra of the molecule, represented in Fig. 7, were recorded to determine the energy position of its ground state, via its first oxidized (HOMO) state, and first reduced (LUMO) states for the three nonequivalent input configurations: (0,0), (1,0), and (1,1). In the HOMO-LUMO gap voltage range small resonances resulting from the superposition of surface states with the Au states appear as shown in Fig. 7. Due to its close proximity to the vacuum level, the LUMO is much broader than the HOMO.[29] This broadening obscures any molecular orbital splitting or shifting obtained when the Au atoms are brought closer to the molecule. On the contrary, the energy shift of the narrow HOMO is clearly observed. As expected from the molecular design, the first oxidation state of the molecule is shifted down when Au atoms interact with the molecule. The output of the logic gate

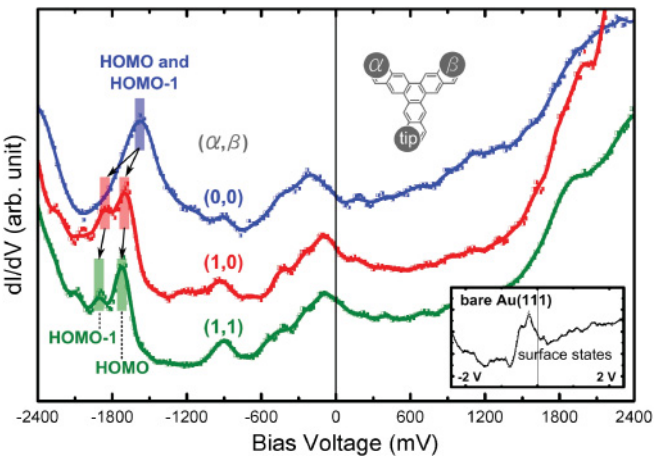

FIG. 7. (Color online) dI/dV spectra for the three nonequivalent Au-trinaphthylene molecule configurations. While a broad peak corresponding to the LUMO appears in all configurations at the positive bias, a distinct peak in the negative regime observed on a bare molecule is split and shifted by Au atom inputs. The HOMO of a molecule in gas phase, with a threefold symmetry, and the degenerated HOMO-1 and HOMO-2 orbitals, with twofold and mirror symmetries, are very close to the same energy level. However once adsorbed on a substrate this degeneracy unravels due to symmetry constrains resulting in the HOMO-2 orbital being dropped out from this energy range. Therefore the peak at −1600 mV in the spectrum taken from a bare molecule consists of only HOMO and HOMO-1. The surface state of Au(111) is provided as a reference.

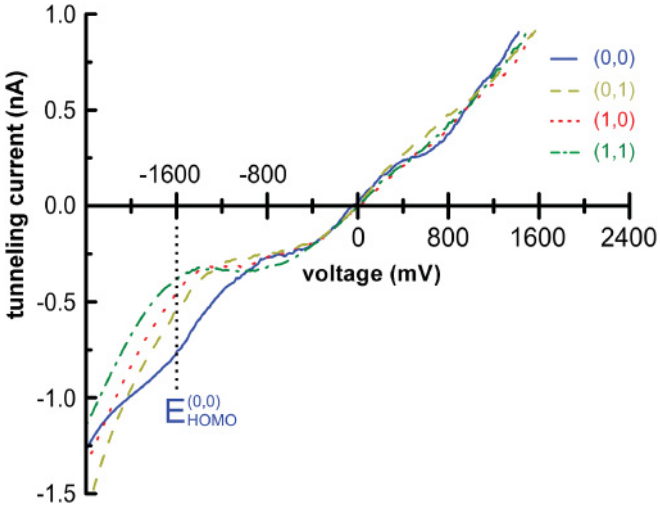

FIG. 8. (Color online) I-V characteristics recorded by positioning the tip apex at the output side of the molecule exactly at the maximum lobe position of the first resonance at negative bias voltage (HOMO). Four I-V characteristics were recorded corresponding to 0, 1, 1, and 2 Au input atoms at the in position. The absolute value of the current intensity is larger in the (0,0) case than in the three other case which is the requirement to obtain a NOR gate.

can then be measured by the conductance of the molecule through the third branch for a bias voltage of −1.6 V. A more convenient way to access the output status of the logic gate is to record the tunneling current intensity measured at the fixed bias voltage of −1.6 V. This is equivalent to integrating the dI/dV spectrum from the Fermi energy down to the HOMO resonance of the (0,0) input configuration. As presented in Fig. 8, the current intensity going through the molecule is consequently high ($I \approx 0.8$ nA) in the (0,0) configuration due to the presence of a conducting channel (the HOMO level) in the integration region. Approaching one or two gold atoms from the molecule pushes the HOMO out of the integration region and the current then drops to ≈0.4 nA. This is exactly the truth table of a NOR gate. The difference between a 0 and a 1 logical output is smaller than in the model case presented in the Fig. 3(b) table. This is due to the fact that for simplicity the experiment was performed directly on an Au(111) metallic surface and not on an insulating surface. The 0.32 nm surface height of the board is not enough to minimize the contribution of all the molecular orbitals to the output tunneling current intensity. The output measurement is far from being the one presented in the Fig. 2 model. Progresses in four-probe UHV measurement is opening an experimental path to perform such QHC single molecule logic gates on a semiconductor surface.[30]

IV. A QUANTUM CHEMISTRY INSIGHT

In order to gain insights into the mechanism of the molecular NOR gate presented above, full semiempirical PM6-CI molecular electronic states calculations[31] have been performed. These calculations allow us to follow how the ground and first excited states of the molecule evolve as a function of the number of Au atoms input. Although useful in identifying a given molecule electronic state associated with an observed electronic resonance, the STM-imaged molecular

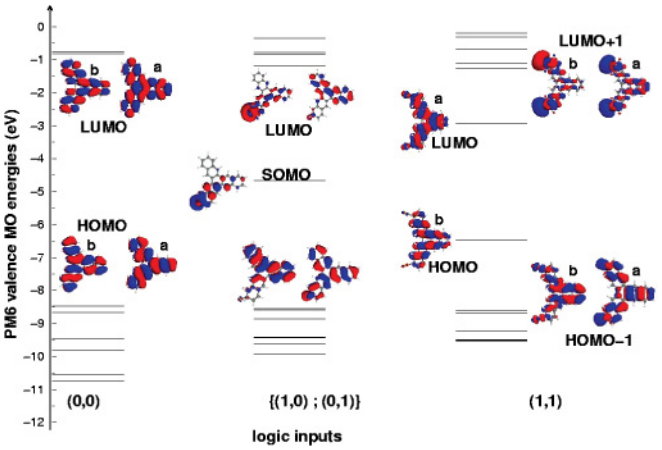

FIG. 9. (Color online) The molecular orbital diagrams of the trinaphthylene molecule for the three different input configurations calculated using the PM6 method. Connecting a Au atom with the molecule deforms its molecular orbitals.

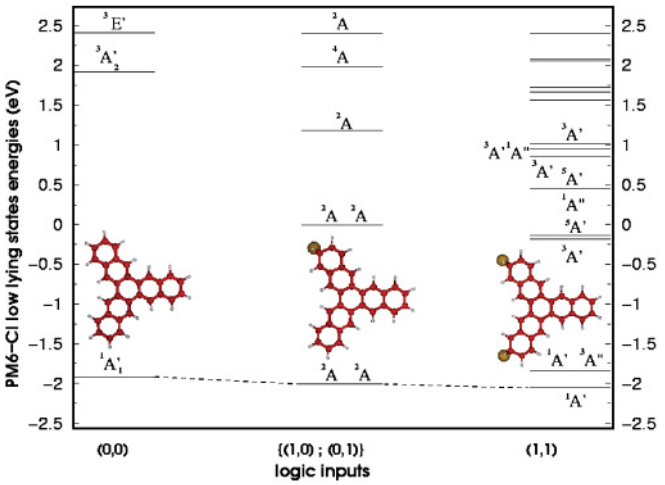

FIG. 10. (Color online) Energy correlation diagram for the ground (1A1) and first excited states of the molecule. Notice how for energies up to the Fermi level the Au interaction spreads the monoelectronic excitation states, many of them being uncoupled from the surface and the tip in an STM junction.

orbitals are only one part of the total description of the electronic states of a molecule. The configuration interaction (CI) calculation allow us to determine the contributions of the different molecular orbitals in a given molecular electronic state, as imaged by the dI/dV STM mapping technique.[29]

Starting from a semiempirical PM6 molecular orbital description of the molecule (see Fig. 9), a multielectronic CI calculation was performed to determine the energetic position of the low-lying valence states for the (0,0), (1,0), and (1,1) configurations. These calculations have been made assuming that the physisorption of the molecule on Au(111) does not shift the energy of its molecular orbitals. The minimum number of self-consistent field (SCF) MOs used in our CI calculations are, respectively, $n = 4$, 5, and 6: the HOMO and LUMO for (0,0), HOMO, SOMO, and LUMO for (1,0), and HOMO, LUMO, LUMO+1, and LUMO+2 for (1,1). More MOs can be added. But the valence states are already stabilized with the ones considered here. The numbers of spin adapted determinants generated by the electronic excitations in the corresponding active space are 36, 100, and 400, respectively. The CI calculations allow us to trace the electronic ground state and the first excited state of the molecule from where the first oxidation and first electronic reduction state will be accessible in a tunneling experiment.

The energy correlation diagram of the lowest valence states [i.e., 3 for (0,0), 5 for (1,0), and 13 for (1,1)], which only involve the monoelectronic excitations belonging to the SCF MOs localized on a trinaphthylene molecule, are presented in Fig. 10. For the (1,0) and (1,1) input configurations, the excitations, picking-up the Au 6*s* atomic orbitals, generate excited electronic states much higher in energy than the low-lying ground and first excited state of the molecule. They can be neglected in a first approximation. The valence states are correlated by their spatial symmetry in the framework of their common C_{2v} subgroup. The CI calculations presented in Fig. 10 confirm that the ground state is shifted down in energy by 0.1 to 0.2 eV when one or two Au atoms are connected to the molecule. This ground state gives rise to the first large electronic resonance observed in the tunneling junction below the Fermi level (see Fig. 6). This is precisely the tunneling resonance which is used to determine the output status of the NOR gate. For the (1,1) input configuration, the triplet state immediately above the ground state had not been observed experimentally even if selection rules do not exist normally for electronic states tunneling spectroscopy.

V. CONCLUSION

In a QHC designed molecule, a logic operation is performed without clustering qubits in the molecule, and it is also not necessary to bind chemical groups like molecular rectifiers, transistors, or switches to construct a logic gate within one single molecule. The local and classical presence of one or two Au atoms on the inputs branches of a trinaphthylene molecule is producing a transformation of its electronic structure readily accessible to tunneling spectroscopy measurements on the output branch. A molecule with a different molecular orbital structure will produce a different Boolean truth table depending on the symmetry breaking of its molecular orbitals upon interacting with the Au inputs and on how those molecular orbitals are mixed up to shape the true molecular valence states. This QHC design can be generalized to more complex logic functions embedded in one molecule creating a definitive link between molecular electronics and quantum design.

ACKNOWLEDGMENTS

We acknowledge the Agency of Science, Technology and Research (A*STAR) for funding provided through the Visiting Investigatorship Program (Phase II) Atomic Scale Technology Project, the European Commission integrated project Pico-Inside, and the MEXT NIMS MANA project. N.R. was supported as part of the Non-Equilibrium Energy Research Center (NERC), an Energy Frontier Research Center funded by the US Department of Energy, Office of Science, Office of Basic Energy Sciences under Award Number DE-SC0000989.

*wh-soe@imre.a-star.edu.sg, n-renaud@northwestern.edu

[1]M. S. M Saifullah, T. Ondaruhu, D. K. Koltsov, C. Joachim, and M. E. Welland, Nanotechnology **13**, 659 (2002).
[2]I. Medalsy, M. Klein, A. Heyman, O. Shoseyov, F. Remacle, R. D. Levine, and D. Porath, Nat. Nanotech. **5**, 451 (2010).
[3]C. Joachim, J. K. Gimzewski, and A. Aviram, Nature (London) **408**, 541 (2000).
[4]C. Joachim, Nanotechnology **13**, R1 (2002).
[5]A. J. Heinrich, C. P. Lutz, J. A. Gupta, and D. M. Eigler, Science **298**, 1381 (2002).
[6]P. Liljeroth, J. Repp, and G. Meyer, Science **317**, 1203 (2003).
[7]E. Meyer and T. Glatzel, Science **324**, 1397 (2009).
[8]A. Imre, G. Csaba, L. Ji, A. Orlov, G. H. Bernstein, and W. Porod, Science **311**, 205 (2006).
[9]J. C. Ellenbogen and J. C. Love, Proc. IEEE **88**, 386 (2000).
[10]L. Lafferentz, F. Ample, H. Yu, S. Hecht, C. Joachim, and L. Grill, Science **323**, 1193 (2009).
[11]F. Remacle and R. D. Levine, Phys. Rev. A **73**, 033820 (2006).
[12]F. Capasso and S. Datta, Physics Today **43**(2), 74 (1990).
[13]J. Chen, M. A. Reed, A. M. Rawlett, and J. M. Tour, Science **286**, 1550 (1999).
[14]M. A. Nielsen and I. L. Chuang, *Quantum Computation and Quantum Information* (Cambridge University Press, Cambridge, 2000).
[15]I. Duchemin, N. Renaud, and C. Joachim, Chem. Phys. Lett. **452**, 269 (2008).
[16]N. Renaud, M. Ito, W. Shangguan, M. Saeys, M. Hliwa, and C. Joachim, Chem. Phys. Lett. **472**, 74 (2009).
[17]C. Joachim and M. Ratner, Proc. Natl. Acad. Sci. USA **102**, 8801 (2005).
[18]N. Renaud, M. A. Ratner, and C. Joachim, J. Phys. Chem. (in press).
[19]J. Bardeen, Phys. Rev. Lett. **6**, 57 (1961).
[20]P. O. Lowdin, Int. J. Quantum Chem. **21**, 69 (1982).
[21]N. Renaud and C. Joachim, J. Phys. A **44**, 155302 (2011).
[22]P. Sautet and C. Joachim, Phys. Rev. B **38**, 12238 (1988).
[23]J. Repp, G. Meyer, S. Paavilainen, F. E. Olsson, and M. Persson, Science **312**, 1196 (2006).
[24]D. Pea, S. Escudero, D. Prez, E. Guitin, and L. Castedo, Angew. Chem. Int. Ed. **37**, 2659 (1998).
[25]C. Romero, D. Pea, D. Prez, and E. Guitin, Chem. Eur. J. **12**, 5677 (2006).
[26]S. W. Hla, K. F. Braun, V. Iancu, and A. Deshpande, Nano Lett. **4**, 1997 (2004).
[27]F. Ample and C. Joachim, Surf. Sci. **600**, 3243 (2006).
[28]F. Ample and C. Joachim, Surf. Sci. **602**, 1563 (2008).
[29]W.-H. Soe, C. Manzano, A. De Sarkar, N. Chandrasekhar, and C. Joachim, Phys. Rev. Lett. **102**, 176102 (2009).
[30]C. Joachim, D. Martrou, M. Rezeq, C. Troadec, D. Jie, N. Chandrasekhar, and S. Gauthier, J. Phys. Condens. Matter **22**, 084025 (2010).
[31]J. J. P. Stewart, J. Mol. Model. **13**, 1173 (2007).